Chapter 6-System Stability Analysis

The last two chapters described how input/output relationships were created for the two major components of the entire system, those being the acoustics and flame. With the addition of a time delay and scaling between each element the entire system can be assembled to complete the stability analysis. A block diagram of the entire system is shown in Figure 6.1. The stability analysis will determine the frequencies at which combustion instabilities are expected in the Solar Turbines combustor.

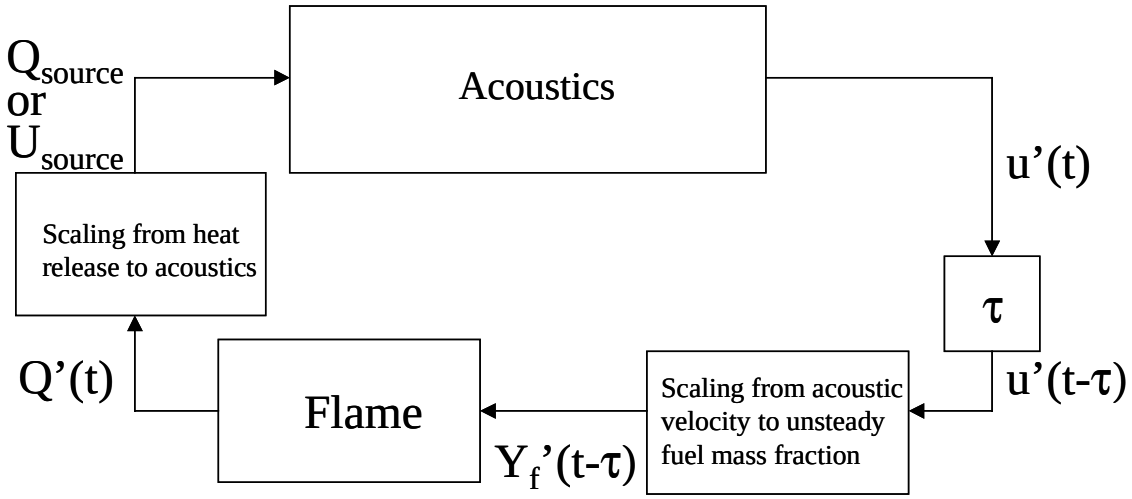

Figure 6.1-Block diagram of entire system.

6.1-Component Assembly

6.1.1-Acoustic Component

Chapter 4 explained how an acoustic transfer function was developed using a 1-D transmission line approach. The frequency response functions (FRF) were an input/output relationship between a voltage input to the speaker and the output acoustic pressure. This relationship was used so that experimental testing could be conducted with a speaker to validate the modeling technique. The actual system, of course, does not receive an input from a speaker but rather it is forced by the rate of unsteady heat release from the flame. Also, the unsteady acoustic particle velocity is the acoustic parameter which drives the flame. The acoustic pressure was the output of the previously discussed models; however acoustic velocity is deterministic when the acoustic pressure wave

amplitude coefficients are known. Figure 6.2 shows the acoustic component of the entire system, with an acoustic source strength input (Q_{source}), and an acoustic particle velocity output u'(t).

Figure 6.2-Acoustic component of entire system.

Through the use of scaling, which will be explained later, the unsteady heat release from the flame can be converted into an acoustic velocity source used to force the acoustics. Equation 6.1 defines the acoustic source strength as the surface integral of the source velocity dotted into the surface's unit normal vector. Therefore, Q_{source} and u_{source} can be used interchangeably given that the appropriate area scaling is used.

$$Q = \int_S \mathbf{u} \cdot \hat{n}\, dS \quad (6.1)$$

In order to introduce an acoustic source strength as forcing to the acoustics, the speaker must be removed. The speaker acts as a dipole velocity source which produces forward and reverse traveling waves which are out-of-phase with each other. The flame acts more like a monopole source in which waves emanate from all directions normal to the source face. The speaker was removed from the previous acoustic models and replaced by an infinitely thin sheet. The volume pulsations of the thin sheet generate in-phase waves. Figure 6.3 shows a schematic of the pulsating volume and the appropriate boundary conditions. As the velocity boundary condition shows, the change in volume velocity across the boundary is equal to the source strength.

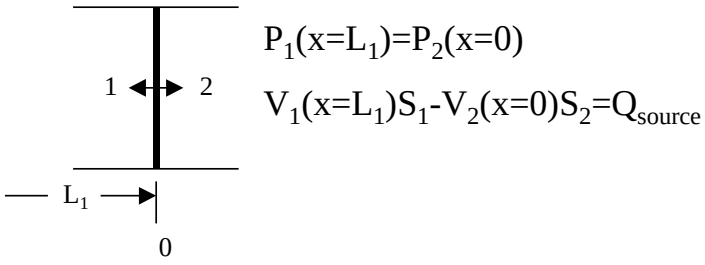

Figure 6.3-Schematic and boundary conditions for monopole acoustic source strength.

With the input converted from a dipole speaker to a monopole source strength, the acoustic output must be converted from acoustic pressure to acoustic particle velocity. As with all fluid systems, velocity is driven by pressure gradients which can be derived using Newton's 2nd Law. Application of this principle yields Euler's equation shown in Equation 6.2 for invisid flows. Euler's equation relates the gradient of the acoustic pressure to the time derivative of velocity. Using this relation provides a means of converting the acoustic pressure to the acoustic particle velocity which is unsteady by definition. Figure 6.4 shows the acoustic FRF for the entire rig with the louver liner. The location where the velocity FRF is calculated is just downstream of the fuel injection location. This is the location where the unsteady velocity causes an unsteady fuel mass fraction which will be convected to the flame front. The source strength input and the unsteady particle velocity output have converted the acoustics into a form which can be incorporated into the entire system.

$$\rho \frac{\partial \mathbf{u}}{dt} = -\nabla p = -\frac{\partial p}{\partial x} \quad (6.2)$$

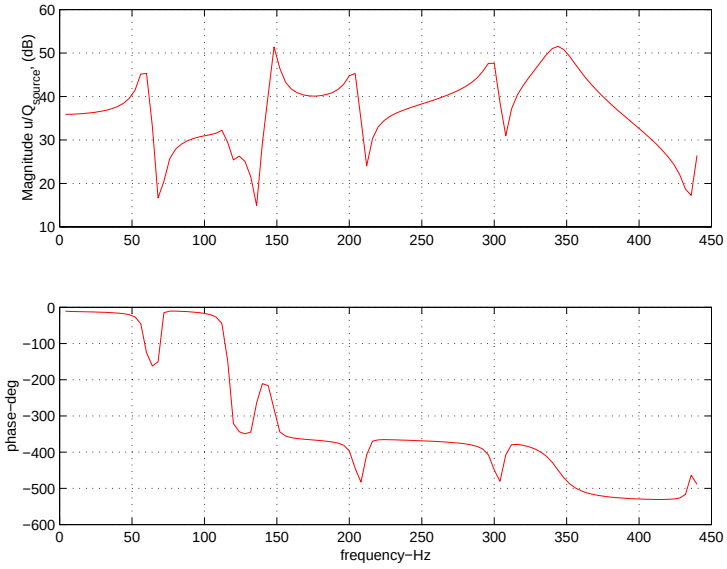

Figure 6.4-Acoustic FRF (u/Q_{source}) of entire rig with louver liner.

6.1.2-Time Delay Component

Time delays occur in systems where there is a delay between an input to the system and the response of the system to that input. Time delays are most common in chemical processes because there is a delay between when the chemicals are injected and when they react. In the combustion system being studying the dominant time delay has been identified as the convective time needed for the fuel to travel from its injection point to the flame front. Figure 6.5 is a block diagram showing that the acoustic particle velocity entering the flame was the acoustic particle velocity at time (t-τ) seconds before.

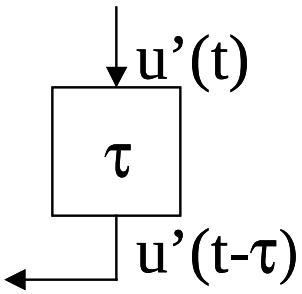

Figure 6.5-Time delay component of the entire system.

A single time delay system, such as the one being investigated, changes only the phase of the system while not affecting the magnitude. Fannin [5] describes how multiple time delays can change both the magnitude and phase of a system. Multiple time delays can be used to control a system by changing not only the phase crossover frequency, but also lower the gain in critical areas where instabilities are predicted. A detailed analysis of multiple time delays has been omitted here since this system has only a single time delay. Mathematically, the time delay is represented by Equation 6.3. This equation shows that the magnitude of the time delay is always unity, and the phase changes according to the delay time (τ). The delay time is simply calculated as the distance from the injector to the flame front divided by the mean injector velocity. Figure 6.6 shows representative FRF's of two extreme time delays for the combustion test rig being modeled. As the mean velocity increases the time delay decreases, resulting in less additional phase compared to lower mean velocities.

$$\theta = e^{j\omega\tau}, \text{ where } \tau = \frac{d}{u_{inj,mean}} \quad (6.3)$$

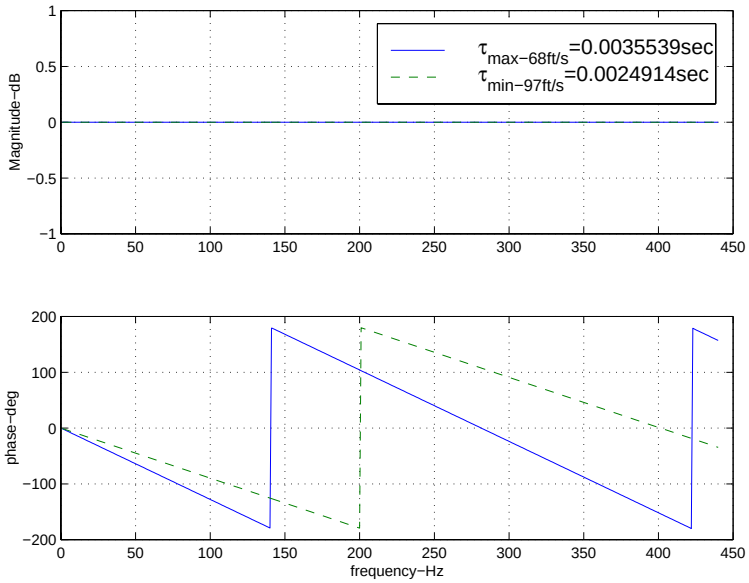

Figure 6.6-FRF of time delay for extreme mean injector velocities.

The time delay component of the system is very important because it provides an easy way to adjust the phase of a system. As will be discussed later, instability occurs when the gain is above 0 dB and the phase crosses 180° for a negative feedback system. By changing the time delay the phase crossing can be moved from an area of high gain (>0 dB), to an area of low gain (< 0 dB). During the design phase the fuel injection location is very easy to change, thus the phase crossing can be moved to obtain more favorable system stability.

The only difficulty associated with the time delay component is determining the correct convective distance needed to calculate τ. The convective distance depends on the location of the flame front, but it is well-known that the combustion process occurs over a finite distance. Therefore, picking a single plane to calculate the time delay can be difficult. The convective distance was chosen based on experimental observations of the flame location within the combustor, and also on which distance provided the best matching between the stability model and the actual instability data taken on the test rig. Another potential problem can occur when the convective distance becomes large. It is

assumed that the fuel/air ratio is frozen between the fuel injector and the flame front, but if the convective distance is long then diffusion must be taken into account. Diffusion would tend to smear out a fuel mass fraction pulse, making the fuel mass fraction much more uniform at the flame front. The test rig modeled by Fannin had multiple fuel injection locations, and at the injector farthest away from the flame it was found that the model was far less accurate in predicting the system's stability. This most likely indicates that the unsteady fuel mass fraction had become smeared due to the long convective length path.

6.1.3-Scaling Between Unsteady Acoustic Velocity and Unsteady Fuel Mass Fraction

Remembering that the input to the flame model is an unsteady fuel mass fraction, some scaling is necessary to convert the acoustic particle velocity into an unsteady fuel mass fraction as shown in the schematic in Figure 6.7. Equation 6.4 shows a derivation of the scaling. Assuming that the fuel line is choked eliminates the unsteady mass flux of fuel. By using the definition of mass flux, the mass of fuel and oxidizer can be related to injector velocity. The only approximation is the Taylor series expansion of the fuel mass fraction in which only the constant and linear terms are retained. The linear equation can then be manipulated to obtain a transfer function relationship between the unsteady inlet fuel mass fraction and the acoustic particle velocity as shown in the last line of Equation 6.4.

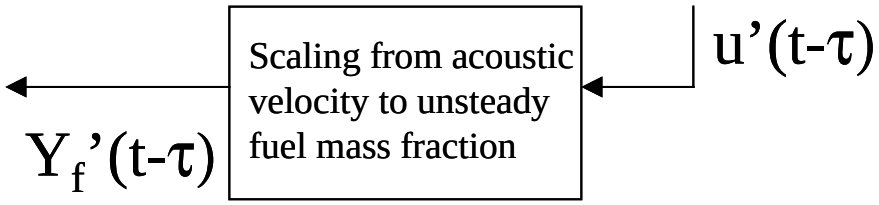

Figure 6.7-Scaling of acoustic particle velocity to unsteady fuel mass fraction.

$$Given: \dot{m}_{oxid,in} = \overline{\dot{m}}_{oxid,in} + \dot{m}'_{oxid,in}\ ,\ \dot{m}_{fuel,in} = \overline{\dot{m}}_{fuel,in} + \dot{m}'_{fuel,in}$$

$$\dot{m}_{oxid,in} = \rho A(\overline{u}_{in} + u'_{in}) = \rho A\overline{u}_{in}(1+\frac{u'_{in}}{\overline{u}_{in}}) = \overline{\dot{m}}_{oxid,in}(1+\frac{u'_{in}}{\overline{u}_{in}})$$

$$Y_{fuel,in} = \frac{\dot{m}_{fuel,in}}{\dot{m}_{fuel,in} + \dot{m}_{oxid,in}} = \frac{\overline{\dot{m}}_{fuel,in}}{\overline{\dot{m}}_{fuel,in} + \overline{\dot{m}}_{oxid,in}(1+\frac{u'_{in}}{\overline{u}_{in}})} = \frac{\overline{Y}_{fuel,in}}{(1+\overline{Y}_{oxid,in}(\frac{u'_{in}}{\overline{u}_{in}}))} \quad (6.4)$$

$$\approx \overline{Y}_{fuel,in}(1-\overline{Y}_{oxid,in}(\frac{u'_{in}}{\overline{u}_{in}}))$$

$$\frac{Y_{fuel,in} - \overline{Y}_{fuel,in}}{u'_{in}} = \frac{Y'_{fuel,in}}{u'_{in}} = \frac{-\overline{Y}_{fuel,in}\overline{Y}_{oxid,in}}{\overline{u}_{in}}$$

In chapter 5 a dynamic flame model was developed to relate an unsteady fuel mass fraction input to an unsteady heat release output. Therefore, no modifications are needed in the model assembly stage.

6.1.4-Scaling Between the Unsteady Heat Release and the Acoustic Source Strength

In order to complete the system loop the heat release must be scaled to force the acoustics as shown in Figure 6.8. Equations 6.5a, b shows two versions of the forced acoustic wave equation. The first equation from Pierce [24] is the acoustic wave equation forced by an acoustic source (Q_{source}), while the second equation from Culick [3] shows how the acoustic wave equation is forced by the unsteady heat release rate. By equating the forcing terms from each equation a transfer function relationship can be derived between the unsteady heat release and acoustic source strength as shown in Equation 6.6. The acoustics are forced by the time derivatives of both the source strength and the unsteady heat release, therefore each must be differentiated with respect to time in order to obtain a transfer function between the actual output of the flame (Q') and the input to the acoustics (Q_{source}). Assuming that the solutions are harmonic, the $j\omega$ term added from the differentiation cancels from both sides of the equation.

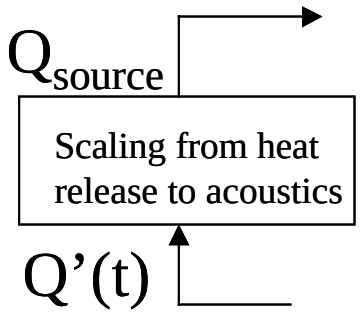

Figure 6.8-Scaling from unsteady heat release to an acoustic source strength.

$$(\nabla^2 + k^2)p = -\rho \frac{Q_{source}}{dt}\delta(x - x_{source})$$
$$(\nabla^2 + k^2)p = -\frac{(\gamma - 1)}{c^2}\frac{dQ'}{dt}\delta(x - x_{source}) \quad (6.5a,b)$$

$$-\rho \frac{Q_{sourve}}{dt} = -\frac{(\gamma - 1)}{c^2}\frac{dQ'}{dt}$$
$$j\omega\rho Q_{source} = \frac{(\gamma - 1)}{c^2} j\omega Q' \quad (6.6)$$
$$\frac{Q_{source}}{Q'} = \frac{(\gamma - 1)}{c^2 \rho}$$

Each block in the system has now been completed and scaled appropriately. The next section will explain how the system was assembled and how the stability analysis was conducted.

6.2-System Stability Analysis

6.2.1-Frequency Response Stability Analysis

In linear system theory, frequency response functions (FRF) show the magnitude and phase of a transfer function as an explicit function of frequency. Once the component transfer functions of a system are assembled, a stability analysis can be conducted based on the gain and phase of the system's open-loop frequency response. Since closed-loop transfer functions maybe unstable or not available for measurements, a FRF response of the open-loop system may be used to determine the stability of the system when the loop is closed. The stability criteria for positive feedback systems can

be simply stated as follows. Frequencies at which the open-loop system has passed through 360° of phase will be unstable if the system gain is above unity (0 dB). The system will be unstable because, if the output is in phase with the input and it amplifies ($|G(i\omega)|>1$) the input, then each time through the loop the amplitude will grow unbounded until non-linear effects become significant. For negative feedback systems, such as the combustion system being studied, the gain criteria is the same but the gain is evaluated when the phase crosses 180°, and not 360° as with positive feedback.

Figure 6.9 shows a block diagram of the system in a form more applicable to performing a stability analysis. Each component of the system now has its own transfer function which when multiplied together forms the composite, or system, transfer function as shown in Equation 6.7. The magnitude of the system transfer function is found by multiplying each of the component magnitudes, while the system phase is found by adding the phase from each component. Based on the analysis from previous chapters, it can be concluded that the acoustics provide most of the dynamic character of the system, meaning that the resonances of the system are very similar to that of the acoustics. It has been shown that the flame acts as a low pass filter which provides gain in the band before its corner frequency. At frequencies substantially higher than its corner frequency the system will never have enough gain ($|G(i\omega)|>1$) to go unstable. The time delay adds additional phase to the system which will change where the system goes unstable. It can also be used as a parameter to move the phase crossings into areas of low gain ($|G(i\omega)|<1$).

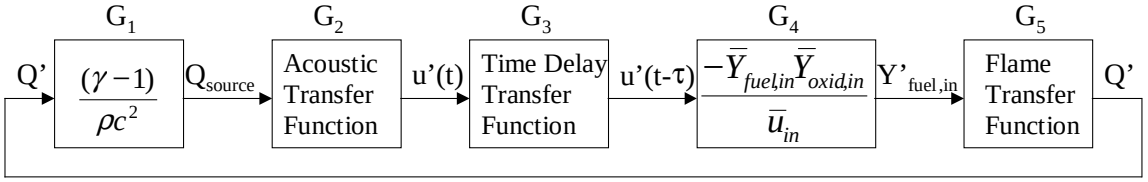

Figure 6.9-Block diagram showing each component of the combustion system with negative feedback.

$$G_{sys}(i\omega) = G_1(i\omega)G_2(i\omega)G_3(i\omega)G_4(i\omega)G_5(i\omega)$$
$$|G_{sys}(i\omega)| = |G_1(i\omega)| \cdot |G_2(i\omega)| \cdot |G_3(i\omega)| \cdot |G_4(i\omega)| \cdot |G_5(i\omega)| \quad (6.7)$$
$$\varphi_{sys} = \varphi_1 + \varphi_2 + \varphi_3 + \varphi_4 + \varphi_5$$

6.2.2-Complete System Frequency Response

Using an acoustic source strength of unity provides an input to the acoustics which filters through each block until the loop has been completed. The resulting open-loop FRF is shown in Figure 6.10. As discussed previously, most of the dynamic content comes from the acoustics, the gain is provided by the flame, and the time delay of 2.2 ms adds the constant negative slope to the system phase. The magnitude plot in Figure 6.10 would indicate that the only chances for instability would be at 55 Hz and 150 Hz, since these are the only locations where the gain is above 0 dB. The magnitude plot also shows that there are many other frequency bands that may have the potential of going unstable if the gain was slightly higher. Therefore, it seems apparent that the system gain is being under predicted. From previous analysis, the flame is known to under predict the unsteady rate of heat release, thus it can be concluded that there must be some additional heat release which would increase the overall system gain. Based on this assumption, the high gain areas will be considered to be above 0 dB in order to determine which frequency bands could be unstable based on the 180° phase crossings.

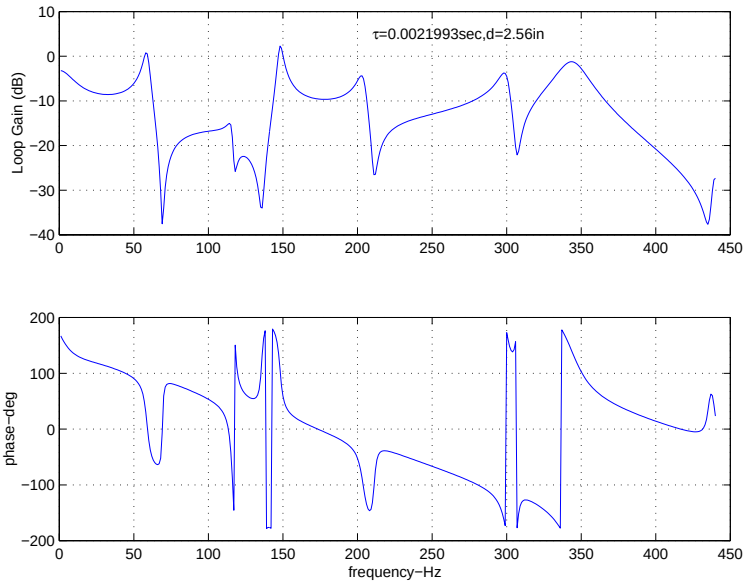

Figure 6.10-FRF of the open-loop single injector test rig system with louver liner at $u_{mean\text{-}inj}$=97 ft/sec and ϕ=.61.

In order to perform a stability analysis using the frequency response function one must first locate where the phase crosses 180°. In Figure 6.10 the phase crossings are indicated by the vertical lines where the wrapped phase jumps from 180° to –180° or vise versa. Phase crossings are seen at 140 Hz, 305 Hz, and 335 Hz. Most of the peaks (poles) of the open-loop system have closely associated nulls (zeros), making the stability of the first two phase crossings difficult to determine. Since the crossings appear closer to the nulls than the peaks they will not be considered instabilities. The 335 Hz phase crossing occurs in a band of high gain, therefore the model would predict an instability at this frequency for the indicated operating conditions. The next section will compare the model's predictions with actual experimental data from the single injector test rig.

6.2.3-Comparison of Experimental Data and Model Predictions

In Figures 6.11-14 power spectrum data taken from pressure transducers in the combustor section of the test rig were compared with the model for the same operating conditions. The experimental data shows that the instability frequency is a strong function of the mean injector velocity with less dependence on the value of the equivalence ratio. In the 22 cases represented by the four power spectrum plots, only two distinct frequency bands near 335 Hz and 240 Hz go unstable. In general, the higher velocity cases produce instabilities near 335 Hz, and the lower velocity cases produce instabilities near 240 Hz.

Comparing the model with experimental data indicates how well the model predicts instability frequencies over a broad range of operating conditions. In general, the model indicates that the equivalence ratio has little affect on the instability predictions. Its only real affect is to slightly change the system gain. The instability frequency is highly dependent on the mean injector velocity. This velocity does very little to affect the magnitude of the response, but through the time delay, it changes where the 180° phase crossing occurs. As the velocity decreases, the time delay increases, adding more phase to the system and lowering the frequency where the phase crossing occurs. As discussed in the previous section for a convective distance of 2.56", and a mean injector velocity of 97 ft/sec, the model predicts an instability will occur near 340 Hz, which is very close to the 335 Hz instability frequency seen in the actual data (Figure

6.11). The phase crossing moves down to ~325 Hz when the mean injector velocity is decreased to 83 ft/sec in the model. This also compares well with experimental data. The only unknown is whether the model would predict a gain high enough to generate an instability since the phase crossing is moving in a direction of decreasing gain from its peak at 340 Hz (Figure 6.12).

When the mean injector velocity is decreased to 78 ft/sec the model does not predict the experimental results as well (Figure 6.13). The model's phase crossing frequency decreases slightly to ~295 Hz, but the experimental results show instabilities at either 320 Hz or 240 Hz. The time delay creates a continuous decrease in the phase crossing frequency, while the experimental data shows only two distinct bands in which instabilities occur. Also, the model would never predict different instability frequencies for the same mean velocity but different equivalence ratios, as the experimental data shows for 68 and 78 ft/sec. When the mean injector velocity is decreased to 68 ft/sec, Figure 6.14 shows that the phase crossing moves down to ~245 Hz based on a convective distance of 2.9". The predicted instability frequency corresponds to the instability frequency seen in the experimental data for some equivalence ratios.

The model seems to predict the general behavior seen in the experimental data. Table 6.1 provides an instability frequency comparison between the experimental data and the model predictions. The biggest discrepancies between the model and the experimental data are as follows:

-The time delay component of the model creates a continuous decrease in the phase crossing frequency as a function of the mean injector velocity, while the experimental data has only discrete instability frequency bands.

-Experimental data indicates that the equivalence ratio can affect where the instability frequency occurs, while the model's prediction of the instability frequency seems completely independent of the equivalence ratio and more a function of the mean injector velocity.

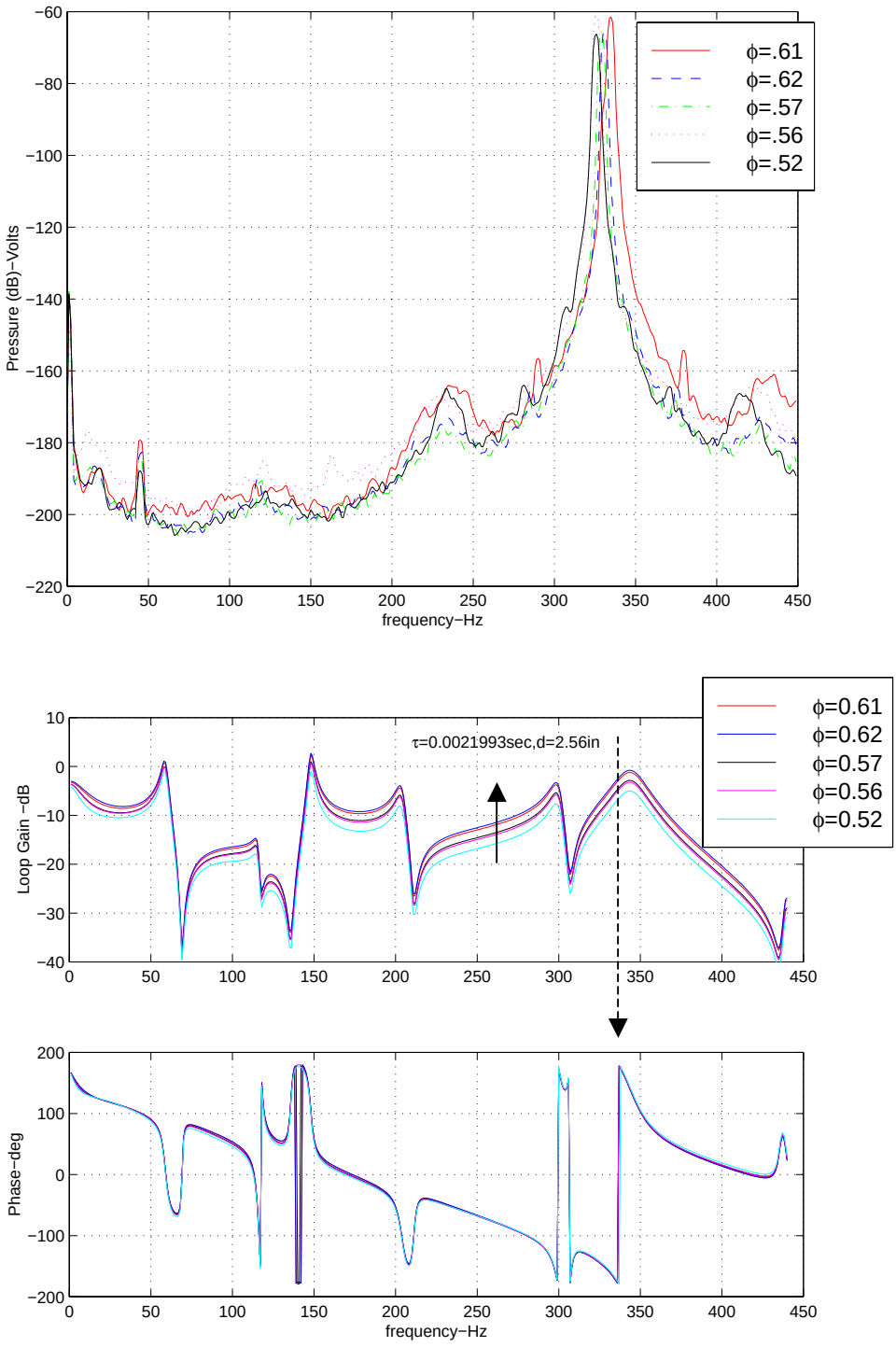

Figure 6.11-Comparison of experimental power spectrum and system FRF model for louver liner with various ϕ and u $_{\text{mean-inj}}$=97 ft/sec. Arrow indicates increasing ϕ. Dashed line indicates instability frequency.

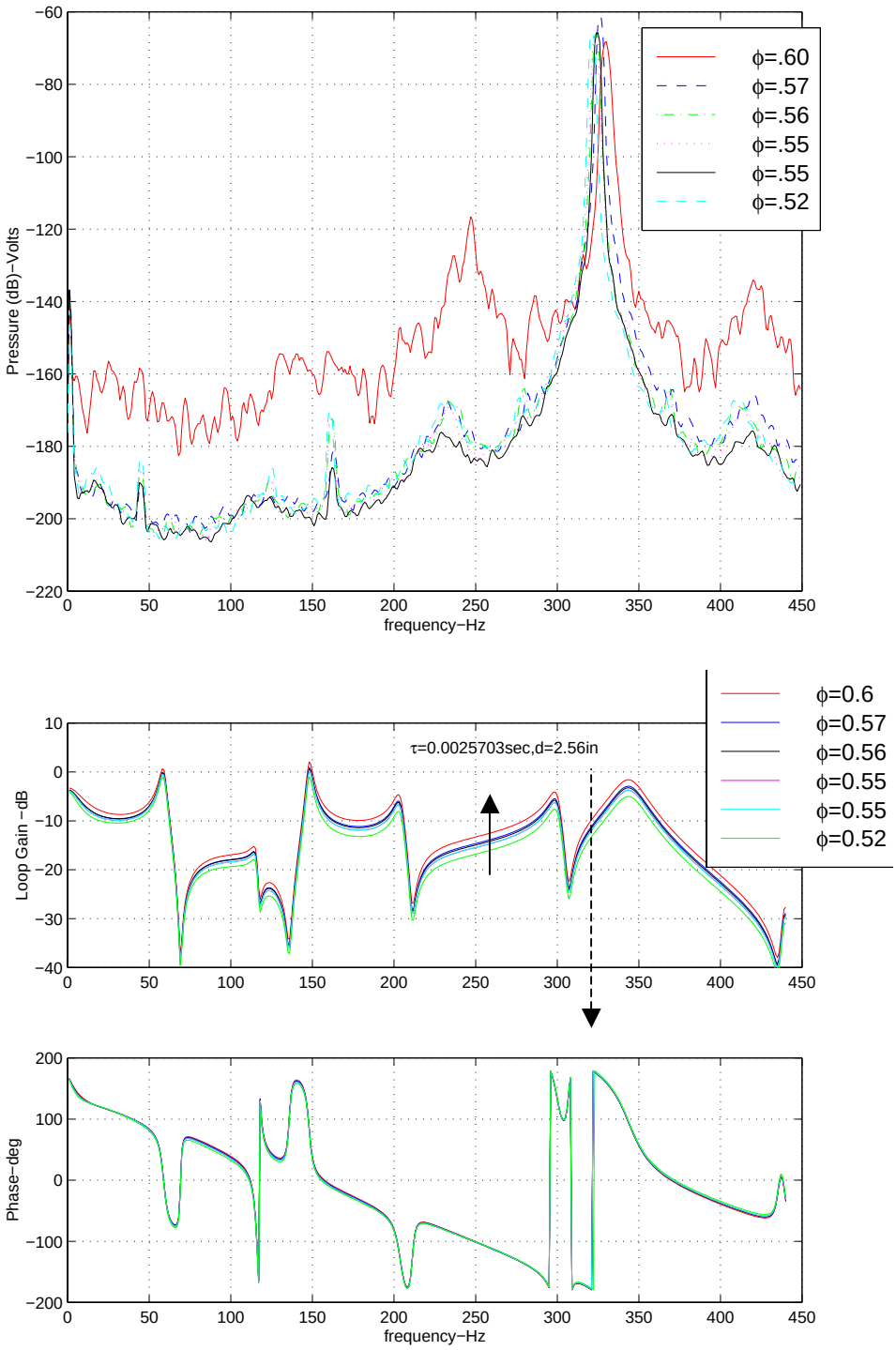

Figure 6.12- Comparison of experimental power spectrum and system FRF model for louver liner with various ϕ and u $_{\text{mean-inj}}$=83 ft/sec. Arrow indicates increasing ϕ. Dashed line indicates instability frequency.

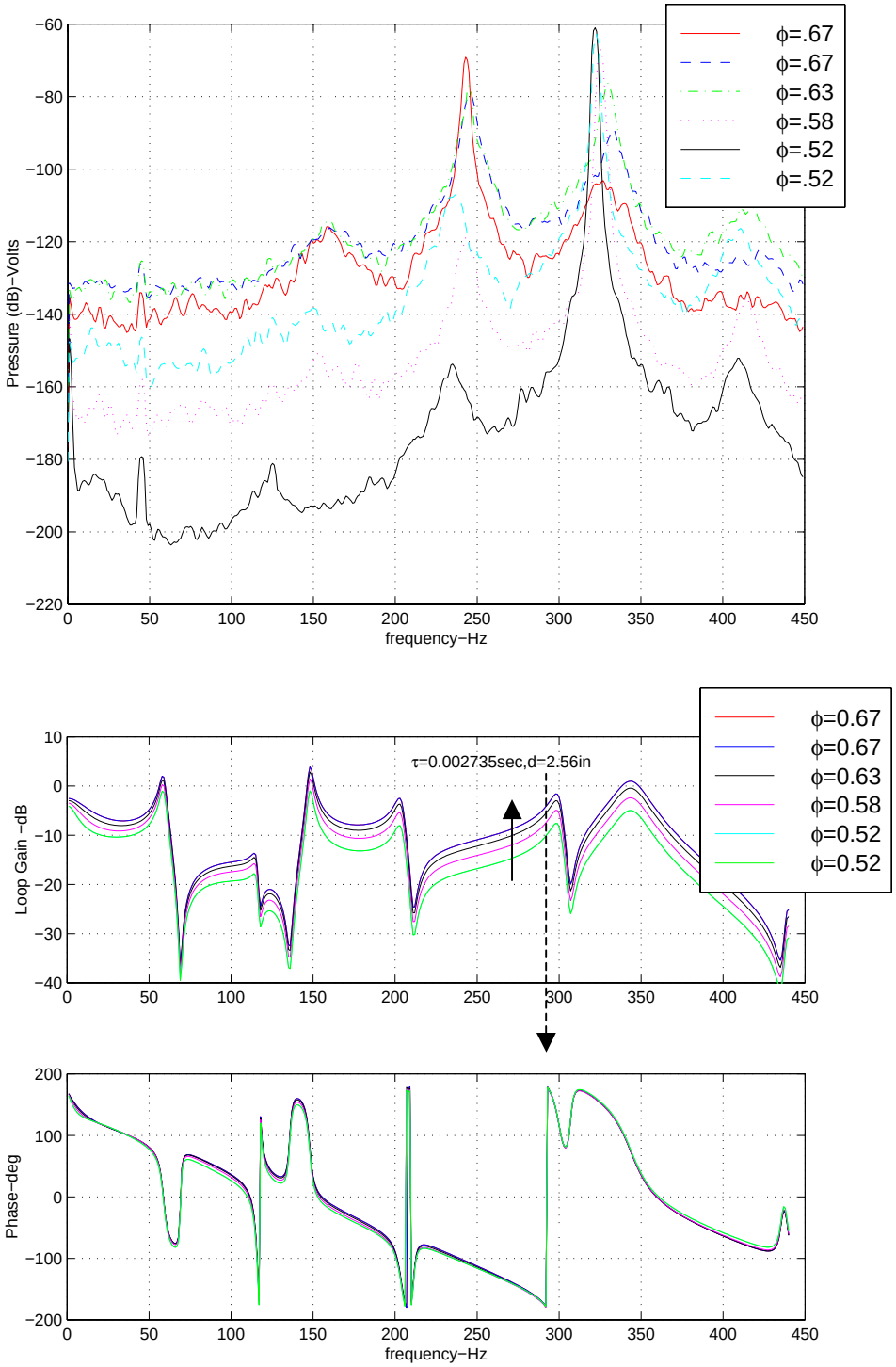

Figure 6.13- Comparison of experimental power spectrum and system FRF model for louver liner with various ϕ and u $_{\text{mean-inj}}$=78 ft/sec. Arrow indicates increasing ϕ. Dashed line indicates instability frequency.

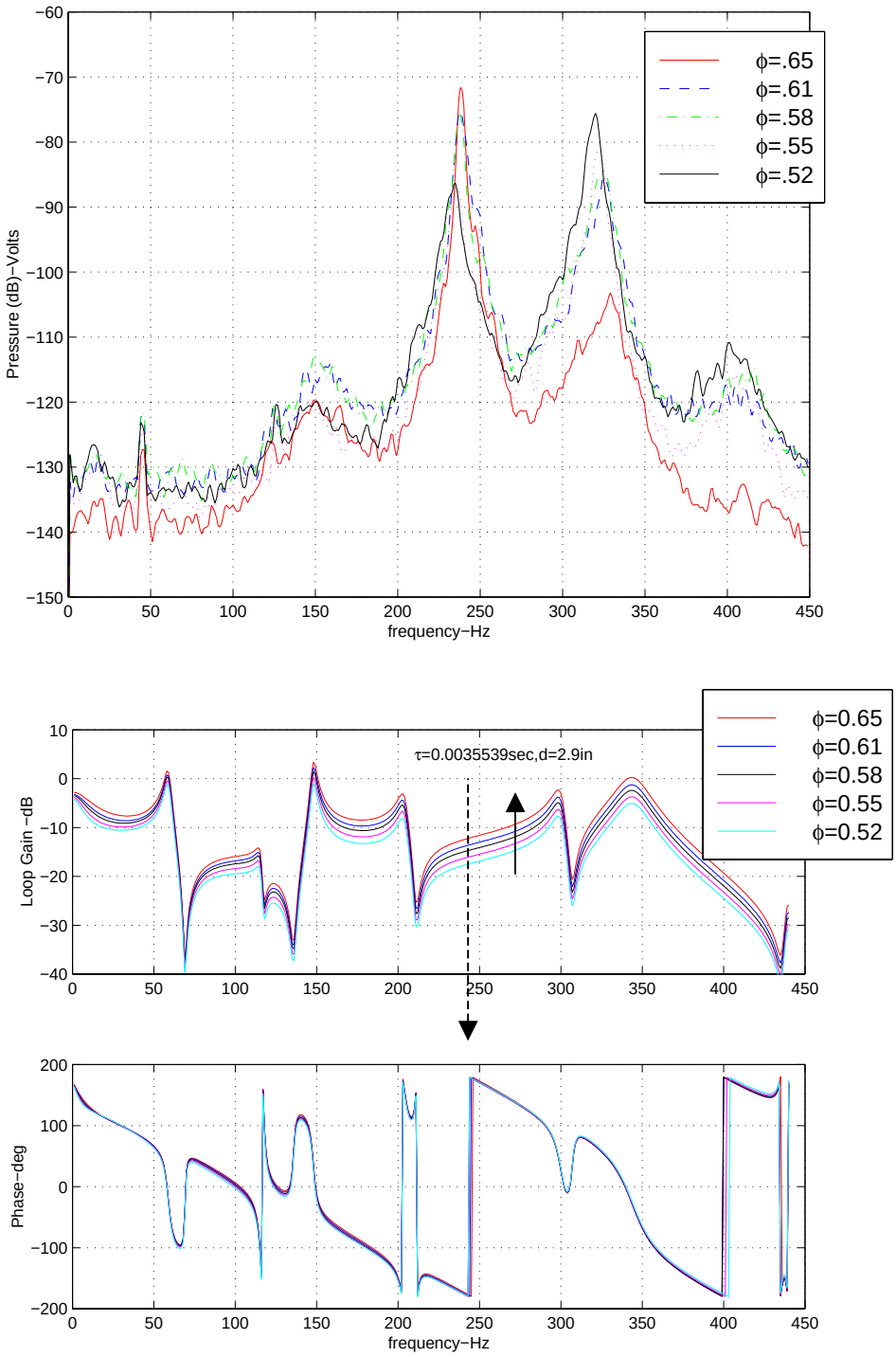

Figure 6.14- Comparison of experimental power spectrum and system FRF model for louver liner with various ϕ and u $_{mean-inj}$=68 ft/sec. Arrow indicates increasing ϕ. Dashed line indicates instability frequency.

Experimental Data			Model Predictions			
$U_{inj\text{-}mean\ (ft/esc)}$	Phi	Instability Frequency (Hz)	Convective Length from Fuel Spokes to Flame Front (in)	180° Phase Crossing Frequency (Hz) (in high gain areas)	Approx. Loop Gain @ Phase Crossing (dB)	Possible Instability Frequency (Hz)
Single Injector Test Rig with Louver Liner						
97	0.61	335	2.56	299, 336	-4.5, -3	299 or 336
97	0.62	335	2.56	299, 336	-4, -2.5	299 or 336
97	0.57	330	2.56	299, 336	-6, -5	299 or 336
97	0.56	330	2.56	299, 336	-6.5, -5.5	299 or 336
97	0.52	325	2.56	299, 336	-8.5, -7	299 or 336
83	0.60	333	2.56	295, 321	-5.5, -3.5	295 or 321
83	0.57	328	2.56	295, 321	-6.5, -5	295 or 321
83	0.56	325	2.56	295, 321	-7, -5	295 or 321
83	0.55	323	2.56	295, 321	-7.5, -5.5	295 or 321
83	0.55	325	2.56	295, 321	-7.5, -5.5	295 or 321
83	0.52	323	2.56	295, 321	-9, -7	295 or 321
78	0.67	243	2.56	206, 292	-7, -4	206 or 292
78	0.67	245	2.56	206, 292	-7, -4	206 or 292
78	0.63	330	2.56	206, 292	-8.5, -5.5	206 or 292
78	0.58	325	2.56	206, 292	-10, -7.5	206 or 292
78	0.52	323	2.56	206, 292	-13, -10	206 or 292
78	0.52	323	2.56	206, 292	-13, -10	206 or 292
68	0.65	240	2.90	202, 244	-3, -12	202 or 244
68	0.61	240	2.90	202, 244	-4, -13	202 or 244
68	0.58	238	2.90	202, 244	-5, -15	202 or 244
68	0.55	323	2.90	202, 244	-7, -16	202 or 244
68	0.52	320	2.90	202, 244	-8, -17	202 or 244
Single Injector Test Rig with Backside Cooled Liner						
87	0.61	315	2.56	272, 315	3.5, -0.5	272 or 315
87	0.56	313	2.56	272, 315	2, -3	272 or 315
87	0.53	313	2.56	272, 315	0, -4	272 or 315
87	0.50	313	2.56	272, 315	-1.5, -5.5	272 or 315

Table 6.1-Instability frequency comparison between experimental data and model predictions for single injector test with louver and backside cooled liner.

In order to gauge the model's ability to predict the dynamic behavior of other system configurations, a model was made for the backside cooled (BSC) liner single injector test rig system. Figure 6.15 shows the FRF of the BSC liner system with a mean injector velocity of 87 ft/sec. A convective distance of 2.56" produced a phase crossing at 315 Hz. This frequency is in a band of high gain and is very near the instability frequency seen in the experimental data. Without experimental data for other mean injector velocities, it is difficult to gauge how accurately the BSC liner system model predicts instability frequencies.

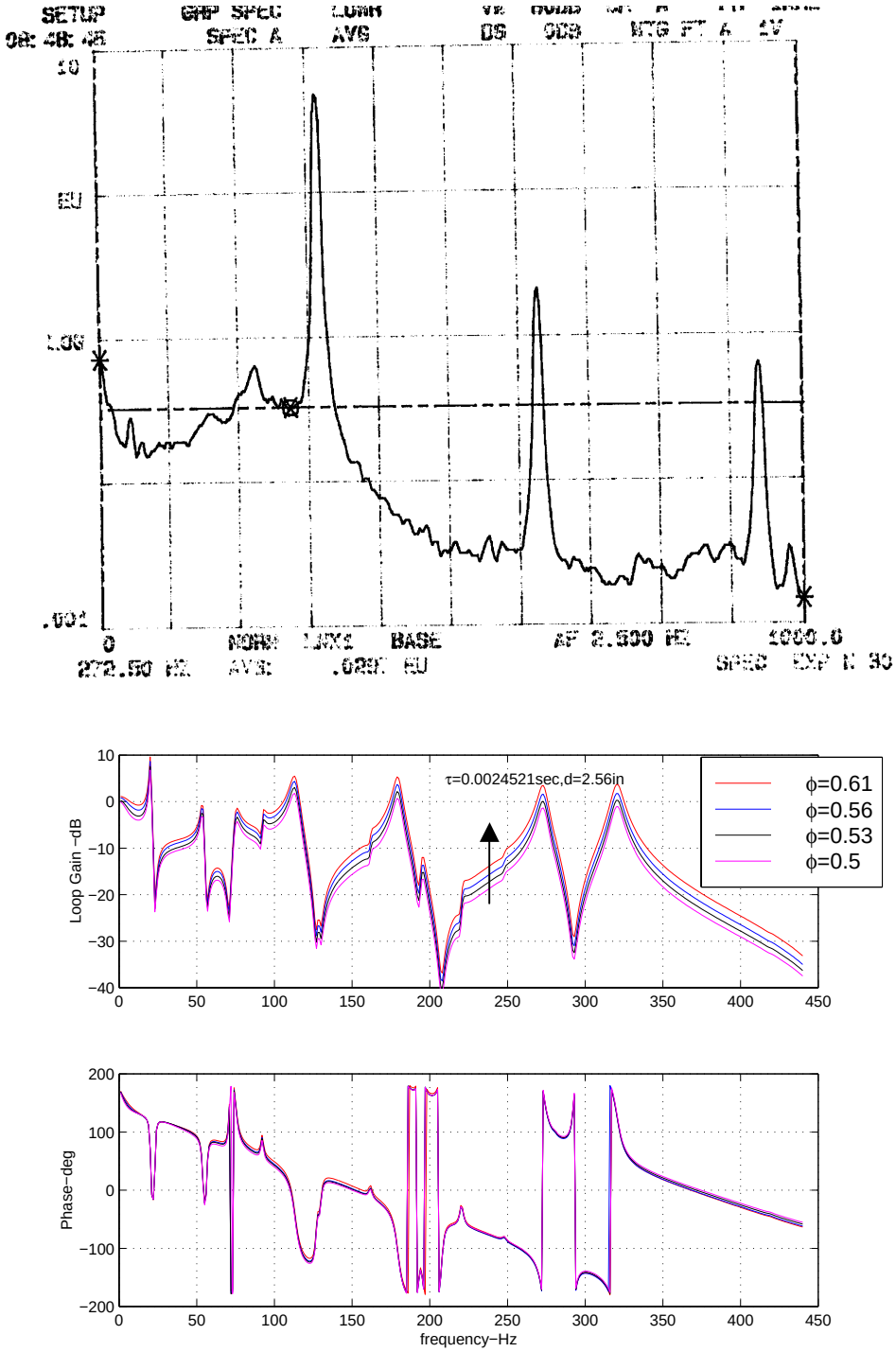

Figure 6.15-Comparison of experimental power spectrum data from 0-1000 Hz and system FRF model for backside cooled liner with various ϕ and $u_{mean\text{-}inj}$=87 ft/sec. Arrow indicates increasing ϕ.

Chapter 7-Conclusions and Future Work

7.1 -Conclusions

The overall goal of this modeling process was to investigate the utility of a linear stability analysis for predicting thermoacoustic instability frequencies in lean premixed combustors. The data presented in the last section, although not conclusive, shows that this analysis technique has the ability to predict instability frequencies for complex combustion systems. The steps used to create the system stability model will provide a methodology for analysis of future designs. This modeling technique provides the user with an adjustable time delay parameter which can be used to avoid potential areas of instability. A single time delay changes the phase crossing frequency, while multiple time delays can act as a notch filter to reduce the gain in specific areas of interest as explained by Fannin [5]. This passive technique can not actively adapt to changing operating conditions, but through a combination of adjusting the magnitude and phase, it may be possible to achieve large frequency bands that are stable for a wide range of operating conditions.

The model, presented in this thesis, was a first-generation model used as a proof of concept. Even though the results are promising, each component of the model must be refined and verified in order to produce a final model which will have the fidelity to make accurate predictions for every operating condition. Listed below are the general conclusions for each component including some of the problems with quantifying their dynamic behavior:

Acoustics:

-One-dimensional acoustic modeling provides accurate results for most of the test conditions. However, there are regions that seem to require more detailed 3-D analysis techniques.

-The acoustic response is controlled by the geometry of the system. Complex boundaries, such as perforates, make accurate predictions of the acoustics much more difficult.

-Simplified acoustic models provide insight into which geometric components dominate the system response.

-The acoustic component of the linear stability model (Figure 7.4) provides most of the system's 'dynamic character'. The resonant response may vary the system gain up to 20 dB at different frequencies.
-The backside cooled liner system model produced much better results than the louver liner system model. This is most likely related to the louver liner's more complex acoustic coupling to the plenum.
-It is difficult to know if the scaling from the room temperature acoustics to the hot acoustics is valid since there is no validation of the hot acoustics.
-The temperature profiles for the hot acoustics decreases the modal density in the bandwidth of interest, resulting in a much more manageable acoustics model.

Single Time Delay:

-The proposed 'equivalence ratio fluctuation' mechanism seems to be supported by reasonable values of time delay for the studied system.
-Time delay adds additional phase lag to the system phase response. The exact time delay value determines where the phase of the system crosses 180°, thus determining the frequency where an instability can occur.
-Time delay provides a control parameter which can be used in the design phase to move potential instability frequencies out of regions with high gain.
-It is difficult to determine the delay distance since it is not known exactly where the heat release occurs. A distributed heat release could result in multiple time delays.

Unsteady Heat Release:

-The unsteady heat release model acts as a low pass filter which adds gain at the lower frequencies and filters out potential instabilities at higher frequencies by reducing the gain.
-The model contributes very little phase to the bandwidth considered here. It mainly adds gain to the system.
-The one-step WSR model is most likely under-predicting the magnitude of the unsteady heat release.

7.2-Future Work

The central problem associated with all of the components in the linear stability model is that there is no way of validating each component. The cold acoustics were validated with experimental data, but there is no easy means of validating the hot acoustics. The convective distance used to calculate the time delay was based only on a visual observation of the general flame location. The flame model was based on an extremely simplified WSR with three species and a one-step reaction mechanism. Future work should be focused on validating each component of the system. A validation procedure involves designing experiments that isolate each model component so that its response can be measured. Below is a list of future work ideas:

Acoustics:

-Design an experiment to excite the acoustics at operating temperature and atmospheric pressure using a speaker that can withstand moderately high temperatures. (~600 K). The atmospheric test rig would be short, thus having only a few resonances in the bandwidth of interest. It would also be easily adjustable so that the resonant frequencies could be changed.

Time Delay:

-An experiment which measures the phase between a fuel pulse input at the fuel injection location and its heat release output is being considered. The goal of this experiment is to calculate the convective distance using the wavelength and measured phase difference of the pulse.

-Designing such an experiment is difficult due to the uncertainties in measuring the heat release. Also, because of diffusion affects the fuel pulse may be somewhat smeared out by the time it reaches the flame front, thus it will be difficult to see a distinct pulse in the heat release.

Combustion:

-Current work is underway to excite a flame with a velocity perturbation and measure its resulting unsteady heat release using OH* correlations, or heat flux gauges. From this data, experimental FRF's can be generated and a transfer function can be fitted to the data. Laminar pre-mixed flames are currently being

studied, with future plans to study gaseous turbulent pre-mixed flames, and liquid fuel flames in a swirl combustor.

Future work will address the validation issue for all of the major blocks needed in the linear stability analysis. With the knowledge gained from these experiments each block will be validated, creating a model which will have the fidelity necessary to predict instability frequencies for any set of operating conditions.